Composites Science and Technology **50** (1994) 355–365

NON-LINEAR NUMERICAL ANALYSIS OF THE IOSIPESCU SPECIMEN FOR COMPOSITE MATERIALS

Henjen Ho,* John Morton

Department of Engineering Science and Mechanics, Virginia Polytechnic Institute and State University, Blacksburg, Virginia 24061-0219, USA

&

Gary L. Farley

US Army Aerostructures Directorate, NASA Langley Research Center, Hampton, Virginia 23665-5225, USA

(Received 6 January 1993; revised version received 6 April 1993; accepted 20 April 1993)

Abstract

A non-linear elastic finite element analysis is presented of the Iosipescu shear specimen tested in the modified Wyoming fixture for unidirectional graphite/epoxy composites. It is shown that the non-linear effects due to specimen-to-fixture contact interactions and specimen geometry on the overall shear response are negligible. It is proposed that the tangential shear modulus should be used to characterize the shear resistance of composite materials with highly non-linear shear response. The correction factors, which are needed to compensate for the non-uniformity of the shear stress or strain distribution in the specimen test section for shear modulus measurement, have to be defined carefully. Strain contours in the non-linear response ranges are presented and the initiation of failure in the notch regions is investigated.

Keywords: non-linearity, numerical analysis, composite materials, Iosipescu specimen, shear modulus, correction factors

INTRODUCTION

The analysis of the mechanical behavior of composite structures requires the stiffness and strength properties of the constituent composite lamina. Of the basic composite mechanical properties, the determination of the shear modulus and shear strength is most difficult and controversial. In the last two decades, a number of shear testing methods for the measurement of shear modulus and shear strength of composite lamina have been proposed and evaluated.[1–7] Among the existing in-plane shear testing methods, the Iosipescu specimen[8] loaded in the modified Wyoming fixture[9,10] is one of the most popular testing procedures[11] by virtue of its unique features.[12] Unfortunately, the Iosipescu shear test is still less than ideal. The main problems associated with the Iosipescu shear test are the non-uniformity of the stress/strain fields in the specimen test section and the combined modes of failure initiated in the vicinity of the notches.[12–15] Numerical analyses[15,16] and experimental full-field moiré interferometry[14] have been performed to evaluate the non-uniformity of the stress/strain fields and calculate the corresponding shear modulus correction factors.[13–16] However, most of the proposed numerical analyses are linear models of the specimen, and there are significant discrepancies in the application of the boundary conditions at the specimen-to-fixture contact regions.[9,10,15–18] Furthermore, the same finite element model has been applied to different specimen configurations even though the material orthotropy is different for specimens with different fiber orientations.[16–18] In a recent study by the authors,[15] equilibrium and compatibility criteria were employed to obtain more realistic linear models of the Iosipescu shear specimens of different fiber orientations and provide an insight into the uniformity of stress/strain distributions in the test section.

In practice, the in-plane shear response of composite materials exhibits severe non-linearity.[19] The non-linearity is attributed to the dominance of the matrix response in the composite shear behavior. Deviation from linearity is observed at small shear strains (e.g. $\gamma_{12} = 0{\cdot}3\%$) for brittle composites and in the early stages of the deformation process for ductile composites (e.g. $\gamma_{12} = 0{\cdot}1\%$) (Fig. 1). However, the non-linear shear response of the Iosipescu specimen could be partly composed of the geometric and

* Present address: Composite Materials and Structures Center, Michigan State University; East Lansing, Michigan 48824, USA.

Composites Science and Technology 0266-3538/94/$06.00

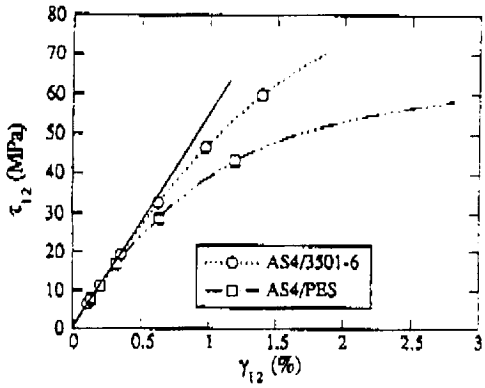

Fig. 1. Typical shear-stress/strain response of 0° AS4/3501-6 and AS4/PES composites from Iosipescu shear test.

boundary contact non-linearities in addition to the material non-linear constitutive behavior. For thermoplastic or metal-matrix composites, plastic behavior of the matrix material largely constitutes the non-linear shear response; therefore, the coupling of shear and extension stresses/strains cannot be ignored.

In this research program, the non-linear shear behavior of AS4/3501-6 graphite/epoxy composite is investigated. A preliminary experimental study showed that the shear response of unidirectional 0° and 90° AS4/3501-6 specimens was non-linear elastic until failure. Owing to the brittle nature of the epoxy resin, the specimen failed before yielding of the matrix occurred so that there was no evidence of matrix plasticity. Thus, the arguments of non-linearity hereafter will be limited to boundary (contact), geometric and elastic material non-linearities.

To investigate the effect of boundary and geometric non-linearity, finite element models of the specimen-to-fixture contacts were employed. The accuracy of the *material* shear-stress/strain data in the non-linear response range were evaluated. In addition, the non-uniformity of the shear-stress/strain fields in the non-linear response range was investigated and the definition of the shear modulus and of shear modulus correction factors are discussed.

The elastic coefficients including those of the non-linear shear constitutive equations are needed in the numerical analysis. Formulations of the in-plane non-linear shear-stress/strain relations have been known for some time. Most of the formulations are based on combined analytical (for example, strain energy function, elastic-plastic flow rule) and experimental (off-axis tensile test) treatments.[19,20] Hahn and Tsai[19] developed a non-linear elastic shear-strain/stress equation for a lamina by adding a fourth-order constant in the complementary strain energy density function. However, the derived third-order shear-strain/stress relation by Hahn and Tsai does not agree with the current experimental results. The one-parameter plasticity model of Sun and Chen[20] does not apply to the brittle material studied in this research. In the current study, an empirical shear-stress/strain relation obtained from the corrected experimental shear-stress/strain curve will be used in the numerical analysis.

FINITE ELEMENT MODELS

The finite element model

When the specimen is secured in the fixture (Fig. 2) the long and short specimen-to-fixture contact lengths are about 31·1 mm (1·25 in.) and 25·4 mm (1 in.), respectively, along the groove and wedge surfaces, (Fig. 3). The distance between the innermost contact region and the notch axis is 7 mm. In most linear models,[9,10,16–18] the modeling of the fixture is ignored, and only the specimen is modeled. In this analysis, the fixture was modeled as four rectangular rigid bodies in contact with the specimen (Fig. 3). The boundary

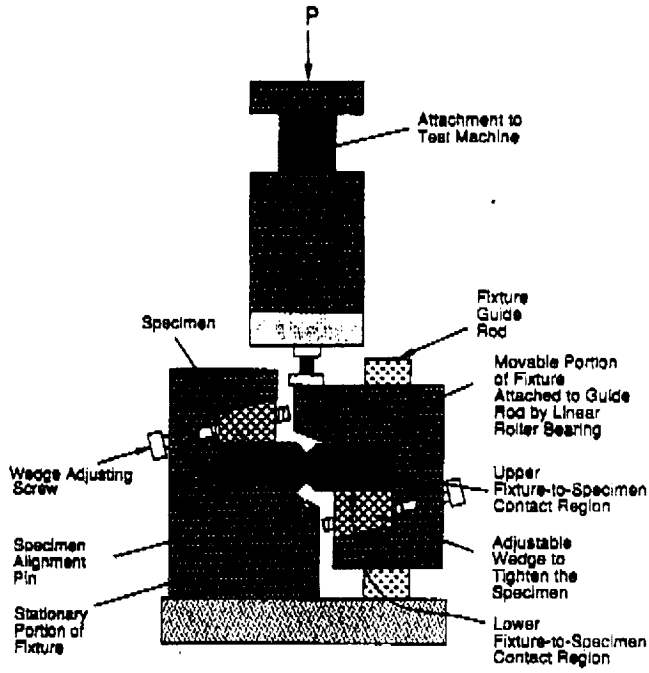

Fig. 2. Iosipescu specimen loaded in the modified Wyoming fixture.

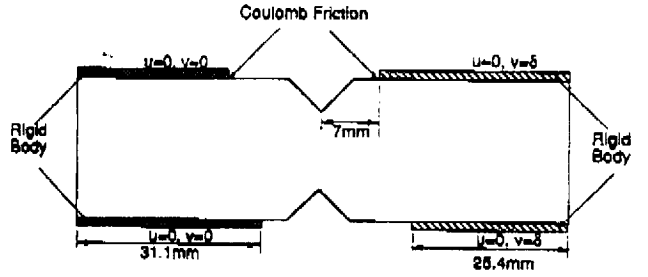

Fig. 3. Finite element model of the Iosipescu specimen tested in the modified Wyoming fixture.

conditions were applied to the four rigid bodies of the fixture. The fixed part of the fixture was modeled into two rigid bodies fixed in space; that is, there is no horizontal and vertical displacement on the fixed part of the fixture. For the movable portion of the fixture, the horizontal displacement was constrained, and a vertical displacement, $v = \delta$, was applied. The magnitude of the vertical displacement on the movable portion of the fixture was adjusted such that the shear strain at the specimen center is equivalent to the failure shear strain obtained from experiment. Along the specimen-to-fixture contact regions, Coulomb friction is assumed. The coefficients of friction in the specimen-to-fixture contact regions are not known *a priori* and are obtained approximately through numerical iterations.

When load is applied, the movable part of the fixture (Figs 2 and 3) moves downward and pushes the right half of the specimen downward along the upper specimen-to-fixture contact region. Thus, load is transferred only from the fixture to the specimen along the upper fixture-to-specimen contact region of the movable portion of the fixture. As the load increases, the specimen may progressively separate from the fixture[15] and the length of the contact region may be reduced. The change of the specimen-to-fixture contact region in the loading process of the specimen is called boundary non-linearity due to the fact that the contact lengths may not be the same at different shear strains of the shear response.

A two-dimensional, plane stress finite element analysis was performed. The finite element mesh in this non-linear analysis is the same as that used in Ref. 15. Along the specimen-to-fixture contact region, contact elements are used. This model had 1468 constant strain elements and 60 contact elements. From the preliminary experimental study, it was found that the specimens failed with small deformations and shear strains, typically $\gamma_{12} \leq 1{\cdot}8\%$. Therefore, the term geometric non-linearity hereafter refers to the non-linearity in the shear response due to the change of specimen geometry.

The constitutive equation

In the non-linear analysis, the most difficult task is the determination of the non-linear constitutive law for the material analyzed. Here, the stress/strain relationships in the longitudinal and transverse directions are assumed to be linear. For the shear behavior, however, a non-linear empirical constitutive law is used. First, a preliminary experiment was performed. The corrected shear-stress/strain curve is obtained by plotting the average shear stress against the corrected shear strain (= measured shear strain multiplied by the reciprocal of the linear shear modulus correction factor[15]). It was found that the constitutive equations corresponding to the modified shear-stress/strain curves for specimens of 0°, 90° and 0°/90° fiber orientations were quadratic functions of the shear strain for a wide range of graphite-reinforced plastics, such as AS4/3501-6, IM8/BMI-PES, and AS4/PEEK.

The iteration scheme

In the numerical analysis, there are two parameters which are not known *a priori*. These are the non-linear constitutive equation and the coefficient of friction in the specimen-to-fixture contact region. Initially, a modified constitutive equation representing the corrected shear-stress/strain curve is used and a very small value of the coefficient of friction is assumed in the specimen-to-fixture contact region. After the analysis is performed, the simulated average shear stress, τ_a, plotted against the gage shear strain (the shear strain calculated over an area equivalent to that of the gage section of the strain gage rosette), γ_g, is obtained. The simulated shear-stress/strain curves are compared to those obtained from the experiments. If the simulated and experimental shear-stress/strain curves do not agree well, small modifications to the coefficient of friction and the second-order term of the constitutive equation are made. The same sequence of steps is repeated until the best agreement between the simulated and experimental shear-stress/strain curves is obtained. It is observed in the simulation that as the coefficient of friction is increased the stress/strain curve shows a tendency to become bilinear. That is, more and more pronounce knee is apparent. The final value of the coefficient of friction is achieved when the simulated shear-stress/strain curve intersects the material constitutive curve at a shear strain higher than the knee in the simulated shear-stress/strain curve.

RESULTS AND DISCUSSION

Comparision of the numerical simulation and experimental result

After several iterations, the simulated and experimental shear-stress/strain curves plotted as the average shear stress, τ_a, against the gage shear strain, γ_g, are shown in Figs 4(a)–(c) for 0°, 90° and 0°/90° specimens, respectively. The corresponding coefficients of friction for 0°, 90° and 0°/90° specimens are 0·3, 0, and 0·2, respectively. For the modified shear constitutive relationship, $\tau = 5{\cdot}0\gamma - 96{\cdot}0\gamma^2$, the shear-stress/strain curves of the numerical simulations and the experimental results agree very well for 0° and 90° specimens (Figs 4(a) and (b)). For the 0° specimen, the linear and quadratic terms of the numerical simulated τ_a–γ_g curve are about 0·7% and 6% different from the coefficients of the experimental τ_a–γ_g curve. For the 90° specimen, the differences in the linear and quadratic terms between numerical

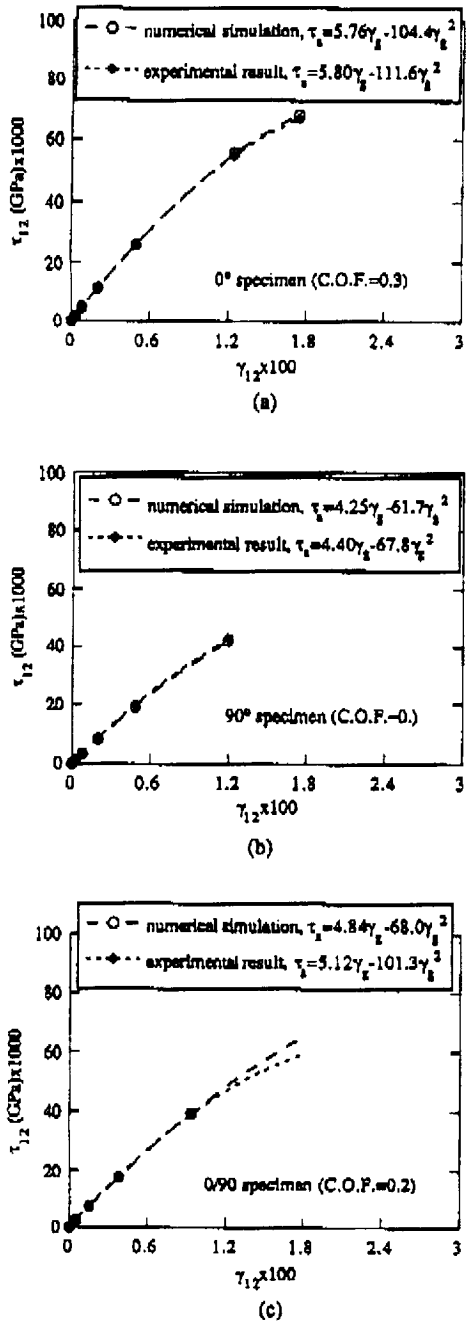

Fig. 4. Shear-stress/strain curves plotted as average shear stress, τ_s, against gage shear strain, γ_g, obtained from numerical simulations and experimental results for (a) 0°, (b) 90° and (c) 0°/90° specimens.

simulated and experimental τ_s–γ_g curves are about 3% and 9%, respectively. For the 0°/90° specimen, poor agreement was obtained when the shear strain is larger than 1·2% (Fig. 4(c)). The linear and quadratic terms in the numerical simulation differ from those from the experimental τ_s–γ_g curves by about 5% and 33%, respectively.

The large difference in the second-order terms for both 0° and 90° specimens may be caused by the variation of the coefficient of friction (non-linear friction) at higher loads due to the change in surface topography of the specimen. Nonetheless, these differences are within experimental data scatter; therefore, no further interations were attempted. The lack of agreement in the numerically simulated and experimental shear-stress/strain curves at large shear strains for the 0°/90° specimen is attributed to interlaminar effects which were not included in the numerical model. The poor agreement between the numerical and experimental shear-stress/strain curves can also be attributed to the material heterogeneity and the damage mechanisms of the cross-ply specimen. Thus, for accurate simulation of shear behavior of the cross-ply specimen, a more complex three-dimensional numerical model is needed. However, due to the laminate nature of the cross-ply specimen, the shear-stress/strain response obtained from the cross-ply specimen cannot be treated as material response. Therefore, further discussion is limited to unidirectional composite laminae with 0° and 90° fiber orientations.

Structural response versus material response

In order to assess the influence of structural parameters upon the shear behavior of the Iosipescu specimen, shear-stress/strain curves obtained from the numerical simulation plotted as gage shear stress, τ_g, against gage shear strain, γ_g, are compared with the input material constitutive curves (Figs 5(a) and (b)). If the output (simulated material behavior) agrees well with the input (material constitutive equation), then the structural effects for this specimen geometry tested in this particular fixture are negligible, and the measured shear-stress/strain curve is the true material response. Conversely, when poor agreement is obtained, the shear response is specimen geometry and fixture dependent (i.e., test method dependent), and the measured shear-stress/strain data are a structural property, rather than a material response. For the 90° specimen, it was found that good agreement between the output (simulated material behavior) and the input (material constitutive response) is obtained. However, for the 0° specimen, the differences between the numerical simulated τ_g–γ_g curve and the input constitutive equation increase with increasing loads. The larger differences between the numerical simulated τ_g–γ_g curve and the input constitutive equation at larger loads for 0° specimen will be discussed in a later section. In general, the 90° specimen provides better agreement between the simulated shear response and the material constitutive response than the 0° specimen.

Force distribution along the specimen-to-fixture contact regions

The degree of non-linearity due to the specimen-to-fixture contact can be evaluated by comparing the

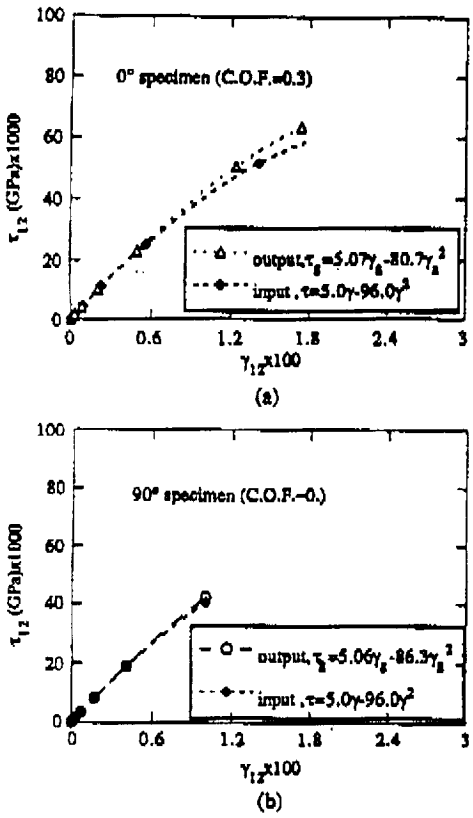

Fig. 5. Shear-stress/strain curves obtained from numerical simulations (τ_g–γ_g) and material constitutive equation (τ–γ) for (a) 0° and (b) 90° specimens.

force distributions along the specimen-to-fixture contact regions in the linear and non-linear shear response ranges. It was found that the lengths of contact are essentially the same in the linear and non-linear elastic (close to failure) range for both 0° and 90° specimens. The distributions of the reaction forces along the specimen-to-fixture contact regions in the non-linear shear response range are shown in Figs 6(a) and (b), which are of similar shape to those in the linear shear response range.[15] The reaction force distributions in the non-linear response range correspond to shear strains of 1·74% and 1·10%, which are the shear strains close to failure for 0° and 90° specimens, respectively. If the lines of action of the equivalent concentrated loads are determined, as shown in Fig. 7, it is found that the distances of the two inner load points, *b*, and the two outer load points, *a*, are essentially the same in the linear and non-linear shear response ranges for the 90° specimen. However, the load points vary slightly in the linear (γ_g = 0·029%) and non-linear (γ_g = 1·74%) shear response ranges for the 0° specimen. The implication of the fixed equivalent concentrated load points in the entire shear response range is that the boundary contact non-lienarity is insignificant.

The difference in the equivalent concentrated load points for 0° and 90° specimens is attributed to the difference in the transverse stiffnesses of the

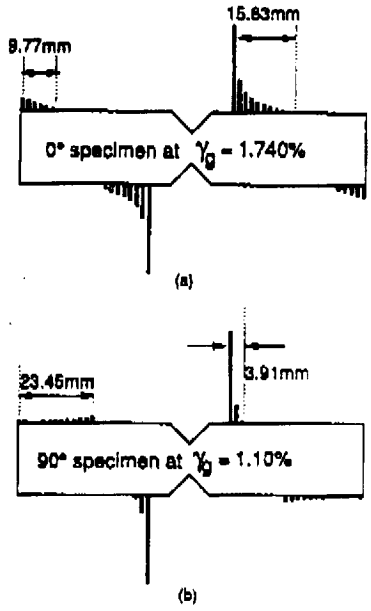

Fig. 6. Schematic distributed forces along the specimen-to-fixture contact regions in the non-linear shear response range for (a) 0° and (b) 90° specimens.

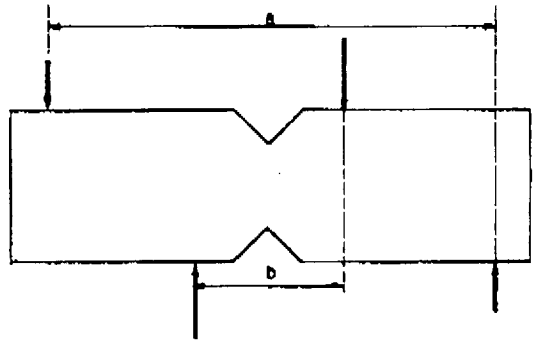

EQUIVALENT LOAD POINTS

	γ_g (%)	a(mm)	b(mm)
0°	0.029	69.24	21.47
	1.74	72.85	22.02
90°	0.026	43.53	16.48
	1.10	43.35	16.50

Fig. 7. Equivalent concentrated load points for 0° and 90° specimens.

specimens. In the 90° specimen for which the transverse stiffness is high, the distance between the two outer load points is about 60% of that of the 0° specimen. Thus there is about 40% excess (unnecessary) material in the standard (76.2 mm, or 3 inch, in length) 90° specimen. It has been shown that the length of the 90° specimen can indeed be reduced[21] without loss of accuracy in the shear modulus and strength measurement.

Effect of frictional forces

In the specimen-to-fixture contact regions, frictional forces develop after the load is applied. Coulomb friction froces are proportional to the applied forces. The coefficients of friction determined from numerical interactions for 0° and 90° specimens are 0·3 and 0,

DISTORTION OF FIBER ORIENTATIONS

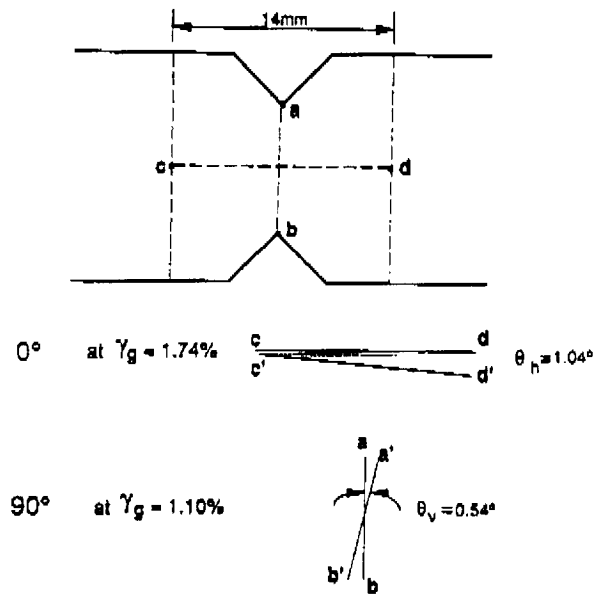

Fig. 8. Simplified schematic diagram of the maximum distortion of fibers in the specimen test section in the nonlinear shear response range for 0° and 90° specimens.

respectively. The effect of frictional forces on the shear stress values in the specimen test sections can also be determined through numerical analysis. It was found that in the test section of the 0° specimen, the shear stress, τ_s, produced by the frictional force is about 0·49% of P/A (P = applied load, A = cross-sectional area) when the gage shear strain is 0·028%, and τ_s is about 0·9% of P/A when the gage shear strain is 1·74%. For the 90° specimen, there is no frictional force induced shear stress because the coefficient of friction is apparently zero. Thus, the effect of the frictional forces on the test-section shear stress is negligible for 0° and 90° specimens.

Geometric non-linearity

In the process of loading, the specimen geometry may change as the load increases. For the 0° specimen, assuming that the longitudinal fiber parallel to the horizontal line *cd*, where *cd* is the distance of unsupported length of the specimen as shown in Fig. 8, remains straight after deformation occurs, the maximum distortion of the fiber along line *cd* is 1·04° at a gage shear strain $\gamma_g = 1{\cdot}74\%$. Similarly, the maximum distortion angle for a 90° specimen along *ab*, the notch axis, is 0·54° at a gage shear strain $\gamma_g = 1{\cdot}10\%$. Since the fibers do not remain straight after deformation occurs the distortion angles are overestimated. Thus, the effect of geometric non-linearity due to the change of specimen geometry on the shear response of 0° and 90° specimens is negligible.

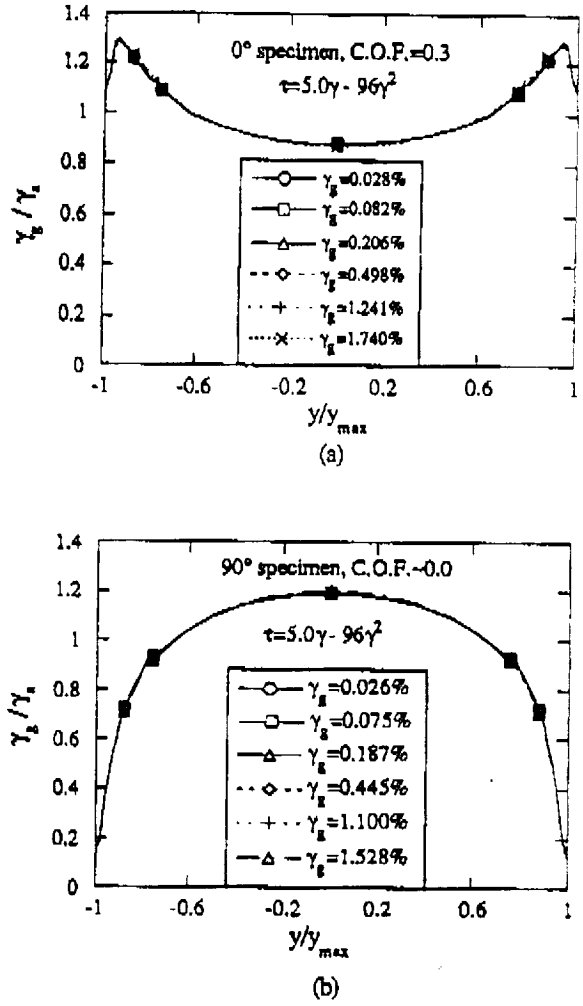

Fig. 9. Shear strain distributions between the notches at several shear strain values for (a) 0° and (b) 90° specimens.

Shear-stress/strain distributions between notches

The shear strain and stress distributions, normalized with respect to the average shear strain and stress in the test section, corresponding to several shear strain and stress values for 0° and 90° specimens, respectively, are shown in Figs 9 and 10. The shear strain distributions at all strain values are essentially the same. This finding is consistent with the previous statement that boundary and geometric non-linearities are negligible. The shear strain distribution across the notches does not become more uniform with the increasing load. However, the shear stress distributions across the test section of 0° and 90° specimens do flatten out with increasing load (Figs 10(a) and 10(b)). The flattening of the shear stress distributions across the test section reflects the non-linear constitutive nature of the materials analyzed. Thus, as the applied load increases, the shear stress concentrations for 0° and 90° specimens are reduced while the shear strain concentrations remain unchanged.

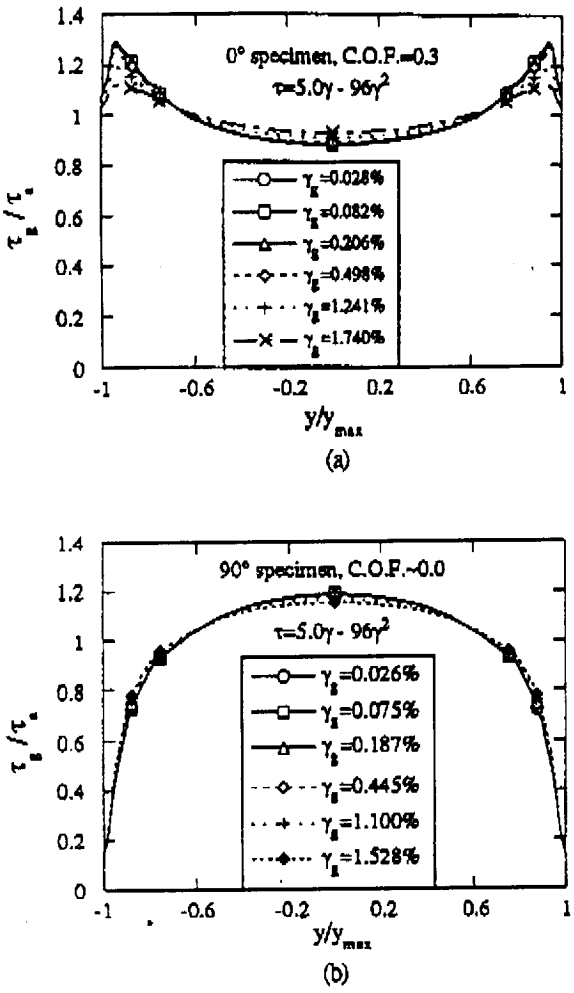

Fig. 10. Shear stress distributions between the notches at several shear strain values for (a) 0° and (b) 90° specimens.

Shear modulus and shear modulus correction factors

In the characterization of the shear resistance of a composite material system, secant, chord, and tangential shear moduli are often used. However, for material systems with highly non-linear behavior, the tangential shear modulus should be used.[22] For example, the tangential modulus at the flat end of a highly non-linear shear-stress/strain curve is nearly zero. The secant and chord moduli at the strains corresponding to the flat end of a shear-stress/strain curve are, of course, not zero.

In common practice, the shear-stress/strain curve obtained from experiment is plotted as the average shear stress, τ_n, across the test section of the specimen against the gage shear strain, γ_g. Therefore, the measured tangential shear modulus, $G^* = d\tau_n/d\gamma_g$, is an apparent modulus. To calculate the shear modulus of the material, either the gage shear strain, γ_g, over the area of a strain gage rosette must be transformed to the average shear strain, γ_n, across the test section; or the average shear stress, τ_n, across the test section must be transformed to the gage shear stress, τ_g. The transformation factors are called the shear modulus correction factors. Because the shear stress and shear strain distributions in the test sections of the 0° and 90° specimens are different, the corresponding shear modulus correction factors for these two fiber orientations are not the same. Depending on the methods of transformation, the correction factor (CF) is defined as

$$CF = d\tau_g/d\tau_n \quad (1)$$

or

$$CF = d\gamma_g/d\gamma_n \quad (2)$$

If the shear behavior is linear, eqn (1) is equivalent to eqn (2). In general, the shear-stress/strain curve is non-linear; therefore, the shear modulus correction factors calculated from eqns (1) and (2) are not the same, even for specimens of same fiber orientation. The shear modulus correction factors using eqn (1) or (2) plotted against the gage shear strains are shown in Fig. 11 for 0° and 90 specimens, respectively. Note that the correction factors calculated using eqn (1) or (2) are not the same and are not constants for both fiber orientations. However, from the results of the preliminary experiments, the condition that the corrected shear moduli obtained from 0° and 90° specimens should be the same is better satisfied only when eqn (1) is used for the definition of correction factors. An example is given in Table 1 where the apparent and corrected shear moduli corresponding to three shear strain values and using eqns (1) and (2) as correction factors are presented. Approximately, the correction factors for AS4/3501-6 graphite/epoxy using eqn (1) can be expressed as:

0° specimen: $CF = 0{\cdot}8586 + 11{\cdot}85\gamma_g - 228\gamma_g^2$ (3)

90° specimen: $CF = 1{\cdot}1868 - 4{\cdot}027\gamma_g + 62{\cdot}0\gamma_g^2$ (4)

where CF and γ_g are the correction factor and the gage shear strain, respectively. In Table 1, it is seen that the corrected shear moduli from the 0° specimen at three shear strain values are lower than those from the 90° specimen even when eqn (1) is used for the

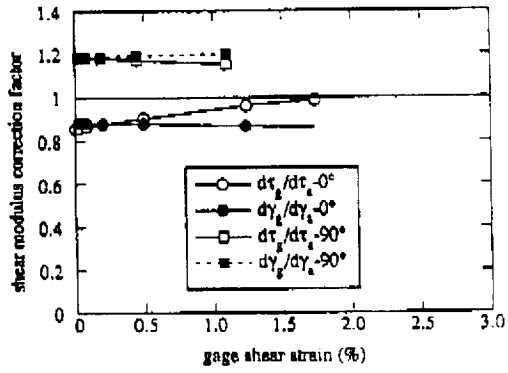

Fig. 11. Shear modulus correction factors for 0° and 90° specimens.

Table 1. Apparent and corrected tangential shear moduli at different shear strains for 0° and 90° AS4/3501-6 specimens

	G_{12}^*(GPa)	$CF = d\gamma_g/d\gamma_a$	$G_{12}^* \times d\gamma_g/d\gamma_a$	$CF = d\tau_g/d\tau_a$	$G_{12}^* \times d\tau_g/d\tau_a$
$\gamma_g = 0{\cdot}2\%$					
0°	5·35	0·884	4·73	0·881	4·72
90°	4·13	1·188	4·90	1·179	4·87
$\gamma_g = 1{\cdot}0\%$					
0°	3·57	0·872	3·11	0·954	3·40
90°	3·04	1·197	3·64	1·153	3·51
$\gamma_g = 1{\cdot}5\%$					
0°	2·45	0·864	2·12	0·985	2·42
90°	2·37	1·202	2·85	1·140	2·70

G_{12}^* is the apparent shear modulus.

correction factors. The lower shear moduli of the 0° specimen are due to its large longitudinal stiffness and the resulting shear induced in the test section by the compressive loads which are attenuated away from the inner load points according to Saint-Venant's principle.[12] Due to this additional shear component, the measured shear strains from the strain gages correspond to a shear stress which is larger than the average shear stress obtained from load cell. As shown in Fig. 5(a), when the shear strain is larger than 1·0%, the gage shear stress (τ_g) is larger than the shear stress (τ) from the material constitutive law. The difference, $\Delta\tau$, may be attributed to the combined increasing effect of the frictional force in the specimen-to-fixture contact region and the (radial) compressive stress attenuated from the inner load points. Therefore, the corrected shear moduli from the 0° specimen are always lower than those of the 90° specimen, especially at large shear strains.

Strain/stress contours and failure initiation

In the specimen test section, the longitudinal normal strain/stress for the 0° specimen and the transverse normal strain/stress for the 90° specimen are of negligible magnitudes due to the large longitudinal and transverse extensional stiffnesses for the 0° and 90° specimens, respectively. The strain contours in the linear response range for 0° and 90° specimens were discussed in Ref. 15. Figures 12 and 13 represent the transverse normal strain/stress and shear strain/stress contours for the 0° specimen at $\gamma_g = 1{\cdot}74\%$ (non-linear response). In the test section, the transverse normal strains, ε_y, are compressive and are about 25% of the magnitude of the shear strains in the test section. At $\gamma_g = 1{\cdot}74\%$, ε_y and σ_y near the notch tips and at the intersections of the notch flanks and notch root regions are both tensile. At the intersections of the notch flank and notch roots the σ_y values are about 45 times the magnitude of those near the notch tips while the corresponding shear stresses at the intersections are about 90% of those near the tips. However, the transverse normal strains, ε_y, at the intersections of the notch flanks and notch roots are about eight times the magnitude of those near the notch tips, and the shear strains, γ_{xy}, are approximately of the same magnitude in these two regions. Nevertheless, due to the large magnitude of the normal stresses (or strains) at the notch flank–root intersections, failure will initiate at the intersections of the notch flank and notch root as observed in the experimental studies.[13,14] Note that even if failure initiates from the notch tips, where the transverse normal stresses (or strains) are tensile at large shear strains, the failure is of mixed mode.

For the 90° specimen, the longitudinal normal strain and stress, ε_x and σ_x, and shear strain and stress contours at $\gamma_g = 1{\cdot}10\%$ (non-linear response) are shown in Figs 14 and 15. The longitudinal normal stresses, σ_x, at the intersections of the notch flank and notch root are about 67% of the maximum shear stress in the test section, while the corresponding shear stresses at the notch flank–root intersections are about 61% of the maximum shear stress in the test section. In terms of strain ratio, the longitudinal normal strains, ε_x, at the intersections of the notch flank and notch root are about 37% of the maximum shear strain in the test section, while the corresponding shear strain at the notch flank–root intersections are about 56% of the maximum shear strain in the test section. Due to the presence of the tensile longitudinal normal strain/stress, the notch flank–root intersections are the potential failure initiation points for the 90° specimen.

CONCLUSIONS

A finite element model for the Iosipescu composite specimen tested in the modified Wyoming fixture accounting for the effect of the specimen-to-fixture contacts has been proposed. The shear responses of the 0° and 90° specimens were simulated numerically to failure shear strains. It was found that the non-linear effects due to specimen geometry and specimen-to-fixture contacts were insignificant for

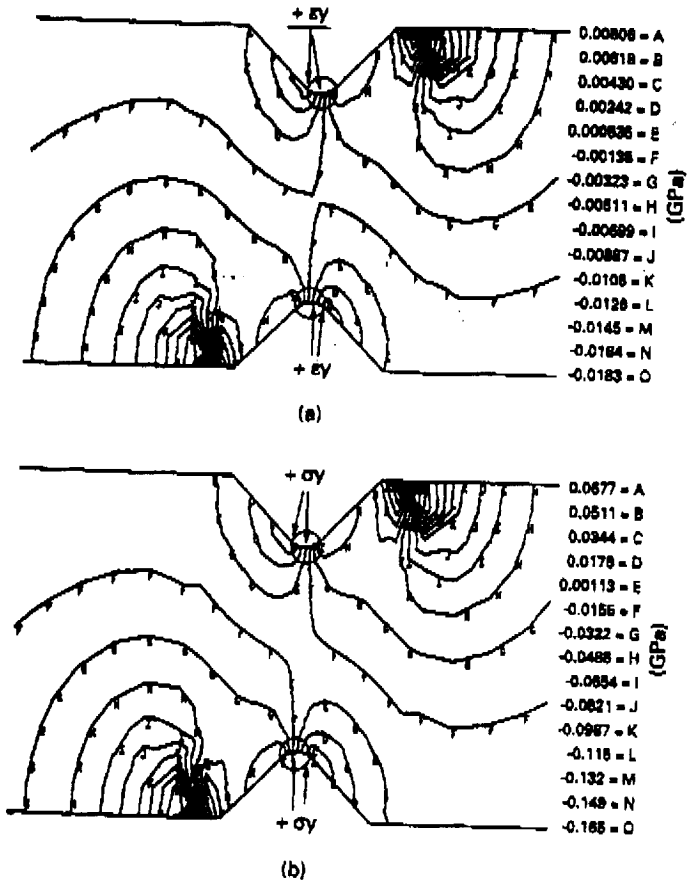

Fig. 12. Transverse (a) normal strain and (b) normal stress contours for a 0° specimen at $\gamma_g = 1{\cdot}74\%$.

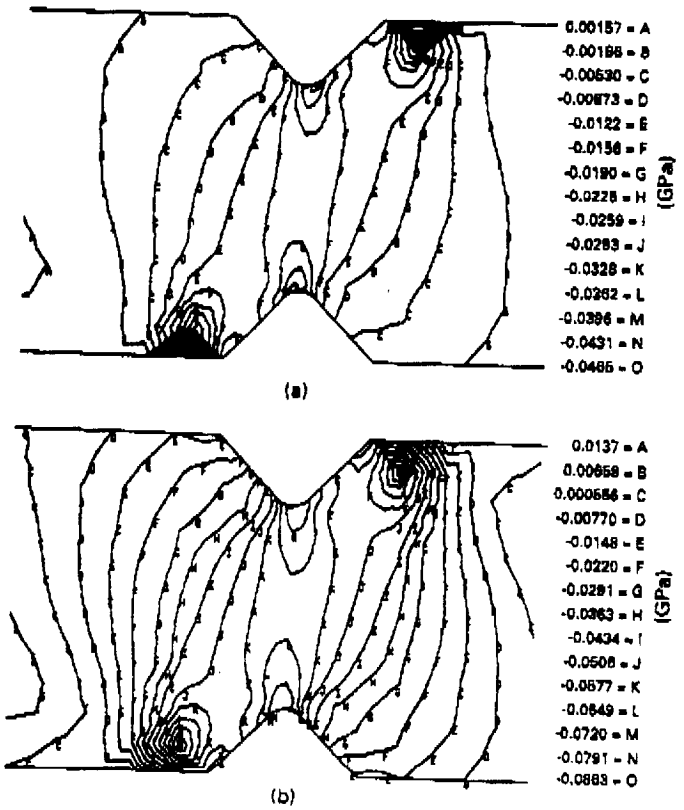

Fig. 13. (a) Shear strain and (b) shear stress contours for a 0° specimen at $\gamma_g = 1{\cdot}740\%$

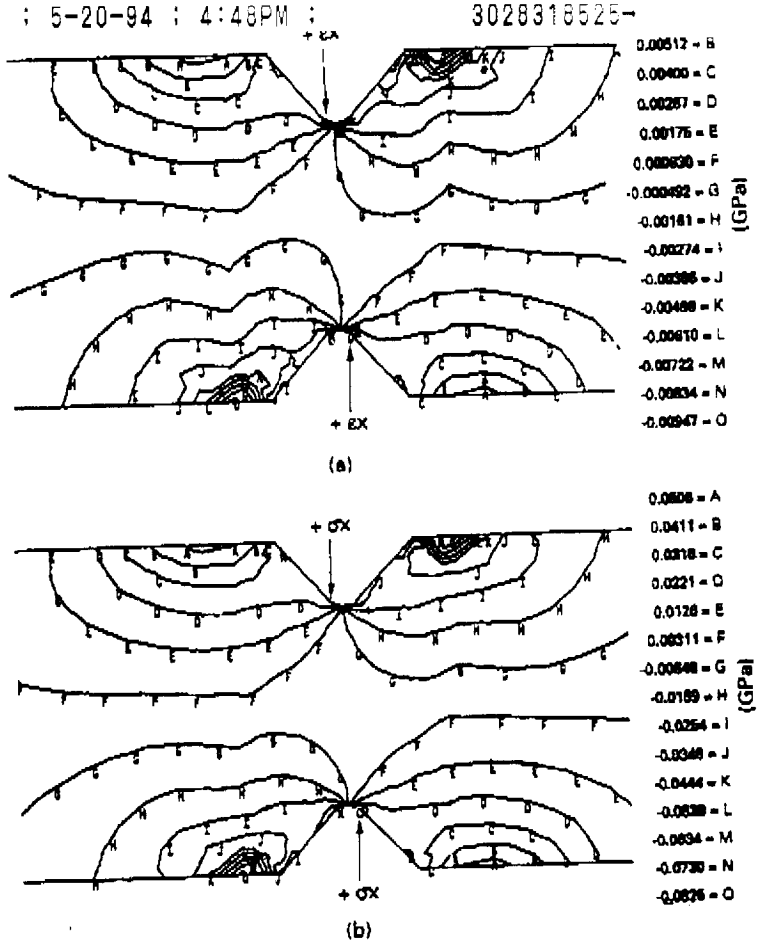

Fig. 14. Longitudinal (a) normal strain and (b) normal stress contours for a 90° specimen at $\gamma_s = 1{\cdot}10\%$.

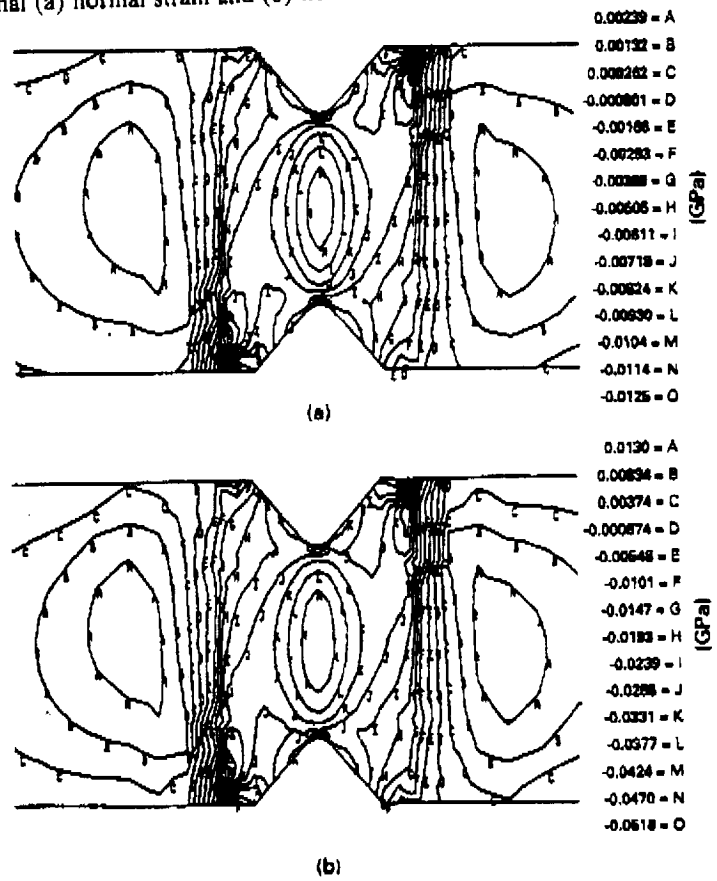

Fig. 15. (a) Shear strain and (b) shear stress contours for a 90° specimen at $\gamma_s = 1{\cdot}10\%$.

both 0° and 90° specimens, though the 0° specimen is more sensitive to the non-linear effect. Numerical simulation of the shear response (τ_s–γ_s curve) for the 90° specimen agrees well with the assumed constitutive behavior. However, due to the proximity of the load points and the large longitudinal stiffness of the 0° specimen, there is an extra shear component associated with a radial compressive stress from inner load points. Therefore, the shear modulus (after application of the correction factor) obtained for 0° specimen will be lower than that for the 90° specimen. In general, the measured shear response for the 90° specimen can be regarded as the material response after proper correction of the measured shear strains.

The normalized shear strain distributions across the notches for specimens of 0° and 90° orientations are essentially the same in the linear and non-linear response ranges. However, the shear stress distributions across the notches for the 0° and 90° specimens became more uniform as the applied load increases. For calculation of the shear moduli in the non-linear shear response regime, tangential shear moduli should be used. To account for the effect of nonuniform shear strain/stress fields on the calculation of the shear moduli, correction factors (CF), defined as $CF = d\tau_s/d\tau_a$, should be applied.

Due to the notch geometry, it was found that the transverse normal strains/stresses for 0° specimen and the longitudinal normal strains/stresses for 90° specimens at the intersections of the notch flank and notch root are tensile; thus, these locations are the potential locations of failure initiation.

ACKNOWLEDGEMENTS

The finanical support of US Army Aerostructures Directorate under NASA Langley Research Center Research Grant NAG-1-1053 and National Science Foundation Science and Technology Center for High Performance Polymeric Adhesives and Composites at Virginia Tech under contract DMR 910024 is greatly appreciated.

REFERENCES

1. Pagano, N. J. & Whitney, J. M., Geometric design of composite cylindrical characterization specimens. *J. Comp. Mater.*, **4** (1970) 538–48.
2. Whitney, J. M., Stansbarger, D. L. & Howell, H. B., Analysis of the rail shear test—Application and limitations. *J. Comp. Mater.*, **5** (1971) 24–34.
3. Petit, P. H., A simplified method of determining the inplane shear stress–strain response of unidirectional composites. ASTM STP 460, 1969, pp. 83–93.
4. Rosen, B. W., A simple procedure for experimental determination of the longitudinal shear modulus of unidirectional composites. *J. Comp. Mater.*, **6** (1972) 552–4.
5. Pagano, N. J. & Halpin, J. C., Influence of end constraint in the testing of anisotropic bodies. *J. Comp. Mater.*, **2** (1) (1968) 18–31.
6. Pindera, M. J. & Herakovich, C. T., Shear characterization of unidirectional composites with the off-axis tension test. *Experimental Mechanics*, **26** (1) (1986) 103–12.
7. Walrath, D. E. & Adams, D. F., The Iosipescu shear test as applied to composite materials. *Experimental Mechanics*, **23** (1) (1983) 105–10.
8. Iosipescu, N., New accurate procedure for single shear testing of metals. *J. Materials*, **2** (3) (1967) 537–66.
9. Adams, D. F. & Walrath, D. E., Further development of the Iosipescu shear test method. *Experimental Mechanics*, **27** (2) (1987) 113–19.
10. Adams, D. F. & Walrath, D. E., Current status of the Iosipescu shear test method. *J. Comp. Mater.*, **21** (6) (1987) 494–507.
11. Lee, S. & Munro, M., Evaluation of in-plane shear test methods for advanced composite materials by the decision analysis technique. *Composites*, **17** (1) (1986) 13–22.
12. Ho, H., Budiman, H. T., Tsai, M. Y., Morton, J. & Farley, G. L., Application of notched beam specimens for shear testing of composite materials. In *Composite Materials: Testing and Design (Vol. 11)*, ed. E. T. Camponeschi Jr. ASTM STP 1206, 1993, (in press).
13. Morton, J., Ho, H., Tsai, M. Y. & Farley, G. L., An evaluation of the Iosipescu specimen for composite materials shear property measurement. *J. Comp. Mater.*, **26** (5) (1992) 708–50.
14. Ho, H., Tsai, M. Y., Morton, J. & Farley, G. L. An experimental investigation of Iosipescu specimen for composite materials. *Experimental Mechanics*, **31** (4) (1991) 328–37.
15. Ho, H., Tsai, M. Y., Morton, J. & Farley, G. L., Numerical analysis of the Iosipescu specimen for composite materials. *Comp. Sci. & Technol.*, **46** (1993) 115–25.
16. Pindera, M. J., Choksi, G., Hidde, J. S. & Herakovich, C. T., A methodology for accurate shear characterization of unidirectional composites. *J. Comp. Mater.*, **21** (12) (1987) 1164–84.
17. Kumosa, M. & Hull, D., FEM analysis of mixed mode fracture in the Iosipescu shear test. In *Proc. 6th Int. Conf. on Composite Materials/2nd Eur. Conf. on Composite Materials Vol. 3*, ed. F. L. Matthews, N. R. C. Buskell, J. M. Hodgkinson & J. Morton. Elsevier Applied Science, 1987, pp. 243–53.
18. Barnes, J. A., Kumosa, M. & Hull, D. Theoretical and experimental evaluation of the Iosipescu shear test. *Comp. Sci. & Technol.*, **28** (1987) 251–68.
19. Hahn, H. T. & Tsai, S. W., Nonlinear elastic behavior of unidirectional composite laminae. *J. Comp. Mater.*, **7** (1973) 102–18.
20. Sun, C. T. & Chen, J. L., A simple flow rule for characterizing nonlinear behavior of fiber composites. *J. Comp. Mater.*, **23** (1989) 1009–20.
21. Budiman, H. T., Ho, H., Tsai, M. Y. & Morton, J., Effect of specimen length and notched geometry on the performance of notched shear specimen. In *Proc. AIAA/ASME/ASCE/AHS/ASC 33rd Structures, Structure Dynamics and Materials Conf.*, Dallas, Part 5, 1992, pp. 2905–14.
22. Zhang, Y. H., Ho, H. & Morton, J., Shear response of a hybrid glass fabric reinforced thermoplastic composite. *Eur. J. Mechan. Eng.* (1992) (submitted).